Waste Management 210 (2026) 115223

Contents lists available at ScienceDirect

Waste Management

journal homepage: www.elsevier.com/locate/wasman

Research Paper

Turning plastic and biomass waste into adsorbents: CO_2/CH_4 separation and comparison with commercial carbons

María Ángeles Martín-Lara *, Mario J. Muñoz-Batista, Gabriel Blázquez, Ledicia Pereira, Alejandra Quintana, Mónica Calero *

Department of Chemical Engineering, Faculty of Sciences, University of Granada, Avda. Fuentenueva s/n, 18071 Granada, Spain

ARTICLE INFO

Keywords:
Co-pyrolysis of waste
Activated carbon production
Carbon dioxide adsorption
Biogas upgrading
Sustainable materials

ABSTRACT

This work compares two commercial activated carbons (CC1 and CC2) with a novel lab-scale activated carbon (NC) produced from the co-pyrolysis of post-consumer plastic waste and olive cake, followed by physical activation with CO_2. The materials were characterized by elemental analysis, proximate analysis, surface area measurements, XRD, and XPS. Elemental and proximate analyses revealed that CC2 possesses the highest carbon content (95.25 %), nitrogen doping (1.62 %), and lowest ash fraction (0.82 %). Textural analysis indicated that CC2 exhibits a high BET surface area (948.55 m^2/g) and micropore area (780.84 m^2/g), while CC1 showed a negligible surface area (2.82 m^2/g), and NC demonstrated a moderate surface area (230.04 m^2/g), indicating a poorly developed porous structure in both cases.

Dynamic adsorption tests showed that CC2 presented the highest CO_2 uptake (up to 2.90 mmol/g) and CO_2/CH_4 selectivity (2.40 in molar terms under biogas conditions), mainly attributed to its well-developed microporosity that favor physisorption. In contrast, NC showed lower CO_2 adsorption (0.80 mmol/g) and higher CH_4 uptake (0.93 mmol/g), resulting in poor selectivity (0.96), suggesting the need for further modification, such as surface functionalization or chemical activation. CC1, limited by its almost non-existent porosity, exhibited intermediate performance with comparable CO_2 and CH_4 uptakes (0.95 and 0.92 mmol/g, respectively) and modest selectivity (1.04), likely influenced by minor chemisorption on mineral impurities.

Despite its lower CO_2 adsorption capacity and selectivity, NC demonstrates high regeneration efficiency, making it suitable for repeated use in gas separation.

1. Introduction

The growing generation of solid waste is a critical environmental concern, driven by population growth and unsustainable consumption patterns (Boules et al., 2024; Bukhari et al., 2025; Seah et al., 2023; Tripathi et al., 2019). Two waste streams of particular concern are agro-industrial residues and post-consumer plastics, both of which are often mismanaged, leading to greenhouse gas emissions and long-term environmental contamination.

Plastic waste poses a major environmental challenge. In 2023, 413.8 million tons of plastic were produced, yet only 8.7 % originated from mechanically recycled post-consumer waste (Plastics Europe, 2024). Approximately 25 % of the generated plastic waste is incinerated, while 55 % ends up in landfills (Lee et al., 2025; Seah et al., 2023).

Olive cake (alperujo), a by-product of the olive oil industry, is another underutilized residue. In 2016, Europe generated approximately 5.5 million tons of olive mill solids (Ferreira et al., 2016; Mechnou et al., 2021). Its low biodegradability and high organic matter content (Aissaoui et al., 2023) generate harmful effects on the environment, as it contributes to phytotoxicity and possesses antimicrobial properties that make its management difficult (Pereira et al., 2024). Traditional methods of managing such waste include incineration and land disposal, which result in the generation of polluting gases and the alteration of the chemical balance of soil and groundwater (Batuecas et al., 2019; Gimenez et al., 2020; Oñate et al., 2024).

Various valorization routes have been proposed for these waste streams, including conversion into biofuels, chemicals, compost, biofertilizers, and bio-based materials. While these strategies offer important benefits, they often require complex processing, high energy input, or face scalability limitations. Adsorbent production emerges as a

* Corresponding author.
E-mail addresses: marianml@ugr.es (M.Á. Martín-Lara), mariomunoz@ugr.es (M.J. Muñoz-Batista), gblazque@ugr.es (G. Blázquez), lpereira@ugr.es (L. Pereira), malejandra@correo.ugr.es (A. Quintana), mcaleroh@ugr.es (M. Calero).

https://doi.org/10.1016/j.wasman.2025.115223
Received 5 August 2025; Received in revised form 7 October 2025; Accepted 31 October 2025
Available online 7 November 2025

particularly promising pathway because it provides a direct, low-energy route to a high-value product from different waste materials. Adsorption technology has been widely used in large number of applications, including water purification to remove pollutants such as heavy metals, organic compounds, pharmaceuticals and other emerging contaminants (Akhtar et al., 2024; Kumar et al., 2021), extraction of metals or other components from complex solutions, such as lithium from brine (Hu et al., 2025a, 2025b) or gas purification (Dan et al., 2024; Guo et al., 2022; Kamran and Park, 2021; Pérez-Huertas et al., 2023; Quan et al., 2023), where the preparation of an adsorbent material with the appropriate characteristics to allow selective adsorption is of great interest, especially in some applications (Hulicova-Jurcakova et al., 2009). Common adsorbents include zeolites, carbon molecular sieves, metal–organic frameworks (MOFs), and activated carbons, which are characterized by high surface areas and tunable surface chemistry through functionalization (Miao et al., 2025; Sidabutar et al., 2025; Yadav et al., 2025). One of the applications that is addressing a pressing environmental challenge is the biogas upgrading (Ashokkumar et al., 2025). By selectively removing CO_2 from raw biogas, adsorbents increase the energy content of biomethane and facilitate a purified product (98 %) suitable for vehicle fuel or injection into the natural gas grid (Peredo-Mancilla et al., 2018).

Among various upgrading methods, adsorption-based processes have been extensively studied to improve the calorific value of biogas and render it suitable for vehicular fuel applications. These methods offer several advantages, including low energy and capital costs, design versatility, operational simplicity, and high separation efficiency (Angelidaki et al., 2018; Augelletti et al., 2017). Adsorption relies on selective gas separation based on the interaction between gas molecules and the active sites of the adsorbent. Common adsorbents include zeolites, carbon molecular sieves, metal–organic frameworks (MOFs), and activated carbons, which are characterized by high surface areas and tunable surface chemistry through heteroatom functionalization that enable high CO_2 adsorption capacity under ambient conditions (Miao et al., 2025; Sidabutar et al., 2025; Yadav et al., 2025).

However, the high cost of some commercial adsorbents has spurred interest in developing low-cost, sustainable alternatives. In this regard, thermochemical conversion technologies such as pyrolysis have emerged as promising strategies for transforming waste into high-value products. Pyrolysis is a thermal decomposition method that converts carbonaceous feedstocks in the absence of oxygen into three fractions: pyrolytic oil, combustible gases, and solid char (Pereira et al., 2024; Seah et al., 2023; Yogalakshmi et al., 2022). Among these, solid char has received comparatively less attention, despite its potential for environmental applications due to its carbon-rich structure.

Recent studies have highlighted co-pyrolysis as an innovative strategy involving the simultaneous pyrolysis of biomass and synthetic waste (e.g., plastics) to produce advanced carbon materials suitable for gas adsorption applications. This approach not only reduces landfill waste and associated emissions but also enhances the properties of the resulting carbon materials. It improves product quality and yield by promoting synergistic interactions between biomass and plastics, often resulting in chars with better hydrogen-to-carbon (H/C) ratio and improved pore structure (Chen et al., 2025; Cupertino et al., 2024; Deng et al., 2025; Hongthong et al., 2024; Patil et al., 2018; Zou et al., 2022).

On this context, this study focuses on the co-pyrolysis of post-consumer plastic waste and olive cake, followed by physical activation with CO_2, to produce a novel activated carbon (NC). The synthesized material was structurally and chemically characterized and compared with two commercial activated carbons (CC1 and CC2). Its performance was evaluated based on CO_2 and CH_4 adsorption capacities under varying concentrations and through multiple adsorption–desorption cycles, aiming to improve biogas quality using a sustainable, low-cost adsorbent. The innovation of this work lies in the combination of two abundant waste streams and their conversion into a functional activated carbon through CO_2 activation, providing a low-cost alternative to commercial adsorbents. In addition, this work offers a direct performance comparison with commercial carbons under dynamic adsorption conditions, enabling a clear assessment of its potential for biogas upgrading.

2. Materials and methods

2.1. Description of the activated carbon materials

The material named as CC1 is a commercial activated carbon of mineral origin extruded in pellet form and physically activated. It is specifically designed for the removal of acid vapors. The particle size is 4 mm, and it has an alkaline impregnation with metals to improve its capacity by a minimum of 8–10 %. The density is 530 g/L. The most common regeneration methods are pressure changes, heating, and purging with an inert gas.

The material CC2 is a commercial carbon molecular sieve developed specifically for gas adsorption in biogas treatment systems using Pressure Swing Adsorption (PSA) or Vacuum Pressure Swing Adsorption (VPSA) processes. It has high stability and a lifespan of 5–8 years, according to the manufacturer. It consists of black cylindrical particles with a particle diameter ranging from 1.3 to 1.8 mm, a diameter vs height ratio of 1:1.5–1:2.0, and can withstand a crushing strength of 90 N. The density is 630–660 g/L. The most common regeneration methods are pressure changes, heating and/or purging with an inert gas, or heating under vacuum, depending on the application. For confidentiality reasons, the companies that produce and supply commercial carbons are not indicated.

The material NC is an activated carbon produced at laboratory scale from a mixture of post-consumption plastic waste and olive cake. Different weight ratios were tested (50–50, 60–40, 70–30, 80–20, and 90–10, always with a higher proportion of plastic waste). Among these, the 50–50 mixture was selected, as prior optimization studies (not shown here) demonstrated that this ratio provided superior pore development. Mixtures with a higher proportion of olive cake were not tested because this residue is available in more limited quantities compared to post-consumption plastic waste. Olive cake was provided by an olive oil mill in the province of Granada, Spain. The olive cake was ground and sieved to remove coarse particles and impurities. The final particle size used was between 2 and 0.25 mm. The plastic waste was provided by the municipal solid waste treatment plant in Granada, Spain, and consisted of a mixture of polypropylene (PP) 55.0 %, high-impact polystyrene (HIPS) 8.6 %, expanded polystyrene (EPS) 10.1 %, and film 27.7 %. The mixture was selected based on the proportion of these materials present in municipal solid waste, which was previously characterized. The dry waste was mixed in the previously indicated proportion and pyrolyzed in a furnace at 500 °C with a heating ramp of 10 °C/min and a residence time of 60 s, under a nitrogen flow of 50 L/h. Subsequently, the resulting char was activated with CO_2, under a heating ramp of 10 °C/min up to 760 °C, maintaining a nitrogen flow of 12 L/h. The char was kept at 760 °C for one hour with a CO_2 flow of 12 L/h. Finally, the activated char was cooled with the same nitrogen flow until room temperature was reached. The activated char obtained was a fine powder with a particle size of less than 0.5 mm.

2.2. Characterization of the activated carbon materials

The proximate analysis was performed using a Perkin Elmer® STA 6000 thermogravimetric analyzer. A portion of the sample was placed in a crucible and subjected to a controlled thermal program under a nitrogen atmosphere (flow rate: 20 mL/min). Initially, the sample was stabilized at 30 °C for 20 min, followed by heating to 110 °C at a rate of 20 °C/min. The temperature was maintained at 110 °C for an additional 20 min to determine the moisture content, calculated from the corresponding mass loss. Subsequently, the temperature was increased to 850 °C at the same heating rate and held for 20 min to quantify the

volatile matter. To assess the ash content, the gas was switched from nitrogen to oxygen (flow rate: 20 mL/min), maintaining the temperature at 850 °C for a further 20 min.

The elemental analysis was quantified in a Thermo Scientific™ CHNS/O analyzer, model Flash 2000. The combustion of the sample at roughly 1400 °C led to the release of CO_2, H_2O, NO_x, and SO_2 gases that were separated in a chromatographic column and detected on a thermal conductive detector. The oxygen content was estimated from the difference between the CHNS content and the ashes.

The textural characteristics of the samples were determined via nitrogen physisorption measurements performed on a Sync 200 apparatus (3P Instruments©). Prior to analysis, all samples underwent degassing at 150 °C under vacuum for 12 h using a Prep J4 unit (3P Instruments©) to remove adsorbed contaminants. Nitrogen adsorption–desorption isotherms were recorded at 77 K. The specific surface area (SBET, m^2/g) was calculated using the Brunauer–Emmett–Teller (BET) method. The micropore surface area (SMP, m^2/g) and micropore volume (VMP, cm^3/g) were derived from the t-plot method, while the total pore volume (VT, cm^3/g) was estimated from the nitrogen uptake at a relative pressure of $p/p_0 \approx 0.99$.

The surface chemical composition was analyzed by X-ray Photoelectron Spectroscopy (XPS) in a Kratos AXIS Ultra-DLD device equipped with an X-ray source from Al Kα. All the spectra were corrected to the C1s peak of adventitious sp3 carbon to 284.6 eV. The deconvolution of the peaks was processed with the aid of the software XPSpeak 4.1®, under a Shirley background correction.

The structural disorder of the carbon material and the presence of crystalline impurities were assessed by X-ray diffraction (XRD) using a Bruker D8 Discover diffractometer equipped with a Pilatus3R 100 K-A detector. Measurements were carried out employing Cu Kα radiation (λ = 1.5406 Å). Diffraction patterns were recorded over a 2θ range of 10° to 85°.

Furthermore, the nature and strength of the surface acid sites were evaluated by Ammonia Temperature-Programmed Desorption (NH_3-TPD) using an AMI-300Lite chemisorption station (Altamira Instruments®) equipped with a Thermal Conductivity Detector (TCD).

2.3. Adsorption-desorption tests in gas phase

Dynamic adsorption experiments for CO_2, CH_4, and their mixtures were carried out in a fixed-bed column setup to obtain breakthrough curves by triplicate. A mass of 1 g of activated carbon was packed into a thermostated column (10 cm in height, 1 cm internal diameter), equipped with a porous ceramic support at the base and operated at 30 °C under atmospheric pressure. Glass beads were placed at the top of the column to minimize solid particle entrainment.

Gas streams composed of CO_2/N_2 or CH_4/N_2 mixtures with volume ratios of 20/80, 40/60, and 80/20 (v/v) were introduced at a constant flow rate of 100 mL/min to determine breakthrough profiles. Additionally, mixed gas adsorption tests were performed using a CO_2/CH_4 mixture of 45/55 (v/v) to simulate a more realistic scenario of biogas upgtrading. The outlet gas composition was continuously monitored using an INFRA.sens® AK5 analyzer (Wi.tec-Sensorik), which operates on a dual-beam non-dispersive infrared (NDIR) detection principle for simultaneous quantification of CO_2 and CH_2. Breakthrough curves were constructed by tracking the outlet gas concentrations over time. The amount of adsorbed CO_2 or CH_4 was calculated as the area under the curve of $1\text{-}C_t/C_{inlet}$, being C_t and C_{inlet} the concentration of the gas at a certain time and the inlet value respectively. The area was computed from the initial time until the saturation time (t_{sat}), defined as the time in which $C_{tsat}/C_{inlet} = 0.95$ (Wang et al., 2015):

$$q = \frac{\vartheta C_0 \int_0^{t_{sat}} \left(1 - \frac{C_t}{C_0}\right) dt}{m_{AD}} \quad (1)$$

where ϑ means the volumetric flow rate (100 L/min), C_0 (mol/L) is the inlet CO_2 or CH_4 concentration, and m_{AD} (g) means the mass of adsorbent loaded in the column.

The adsorption–desorption cycles were carried out by swapping the inlet with pure N_2 at the same flow rate, i.e. 100 mL/min. The desorption cycle was finalized when the monitored CO_2 and CH_4 concentrations were negligible.

The selectivity was calculated from the results of dynamic tests as follows:

$$S_{CO_2/CH_4} = \left(\frac{q_{CO_2}}{q_{CH_4}}\right) \quad (2)$$

where q_{CO_2} and q_{CH_4} is the gas uptake of the component at 298 K and atmospheric pressure.

3. Results and discussion

3.1. Characterization of activated carbon materials

Table 1 summarizes the elemental composition, proximate analysis, and textural properties based on results of N_2 adsorption–desorption isotherms of the two commercial activated carbons (CC1 and CC2) and the developed novel carbon material (NC).

Elemental analysis revealed that the CC2 exhibits a notably higher carbon content (95.25 %) compared to CC1 (67.13 %) and NC (35.79 %), indicating a higher degree of carbonization and purity. Additionally, the CC2 contains more nitrogen (1.62 %) than the other two samples, suggesting the presence of nitrogen-functional groups that could enhance surface reactivity, potentially benefiting applications such as adsorption or catalysis (Biniak et al., 1997; Hulicova-Jurcakova et al., 2009; Jansen and van Bekkum, 1995). Hydrogen content remains consistent for both commercial carbons with a value of 1.91 % and is considerably lower in NC (0.48 %).

Proximate analysis also showed main differences in moisture, volatile matter, fixed carbon, and ash contents. CC2 has the lowest moisture (1.29 %) and ash (0.82 %) contents, along with the highest fixed carbon (93.47 %), indicating superior thermal stability and purity (Sádovská et al., 2023; Zhao et al., 2023). In contrast, NC, shows low fixed carbon (25.48 %) and elevated ash content (44.66 %), possibly due to residual inorganic components from the precursors (plastic and olive pomace). On the other hand, the high volatile matter in NC (21.89 %) compared to commercial materials reflected less intense activation conditions (Jurkiewicz et al., 2023; Pui et al., 2019). Although NC could retain certain chemical groups that might be beneficial for specific adsorption scenarios.

Finally, textural properties assessed by N_2 adsorption–desorption isotherms, further revealed differences into the studied materials. CC2 displays a high BET surface area (948.55 m^2/g) and great microporosity, as indicated by a micropore area of 780.84 m^2/g and a micropore volume of 0.380 cm^3/g. In contrast, CC1 show negligible surface area (2.82 m^2/g) and NC a moderate surface area 230.04 m^2/g, indicating a poorly and low developed porous structure.

As conclusion, from these characterization results, the need for further optimization of activation and post-treatment processes to enhance structural and adsorption properties of CC1 and NC samples and a preliminary good performance of CC2 for adsorption-based applications, due to its most favorable balance of chemical purity and porosity, can be detected.

The characterization of the materials is completed with structural and surface analyses by X-ray diffraction (XRD) and X-ray photoelectron spectroscopy (XPS). The XRD patterns (Fig. 1A) of the three carbons display the hallmark features of turbostratic carbon-namely a broad band in the 20–30° (2θ, Cu Kα) region, assigned to the (002) stacking of disordered graphene layers, and a weaker, broad feature at ~41–46° attributable to the (1 0 0)/(1 0 1) in-plane reflections (Besinella et al.,

Table 1
Elemental composition, proximate analysis, and textural properties of the two commercial activated carbons (CC1 and CC2) and the developed novel carbon material (NC).

Analysis		Commercial activated carbon 1 (CC1)	Commercial activated carbon 2 (CC2)	Novel activated carbon (NC)
Elemental, % (dry basis)	C, %	67.13	95.25	35.79
	H, %	1.91	1.91	0.48
	N, %	0.17	1.62	0.21
	S, %	0.00	0.00	0.00
	O, % (by difference)	16.31	0.39	15.00
Proximate, % (wet basis)	Moisture, %	16.53	1.29	7.96
	Volatile matter, %	13.22	4.42	21.89
	Fixed carbon, %	58.16	93.47	25.48
	Ashes, %	12.09	0.82	44.66
N_2 adsorption–desorption isotherms	BET surface area, m^2/g	2.82	948.55	230.04
	t-plot micropore area, m^2/g	3.69	780.84	148.63
	Total pore volume, cm^3/g	0.009	0.524	0.123
	t-plot micropore volume, cm^3/g	0.002	0.380	0.075

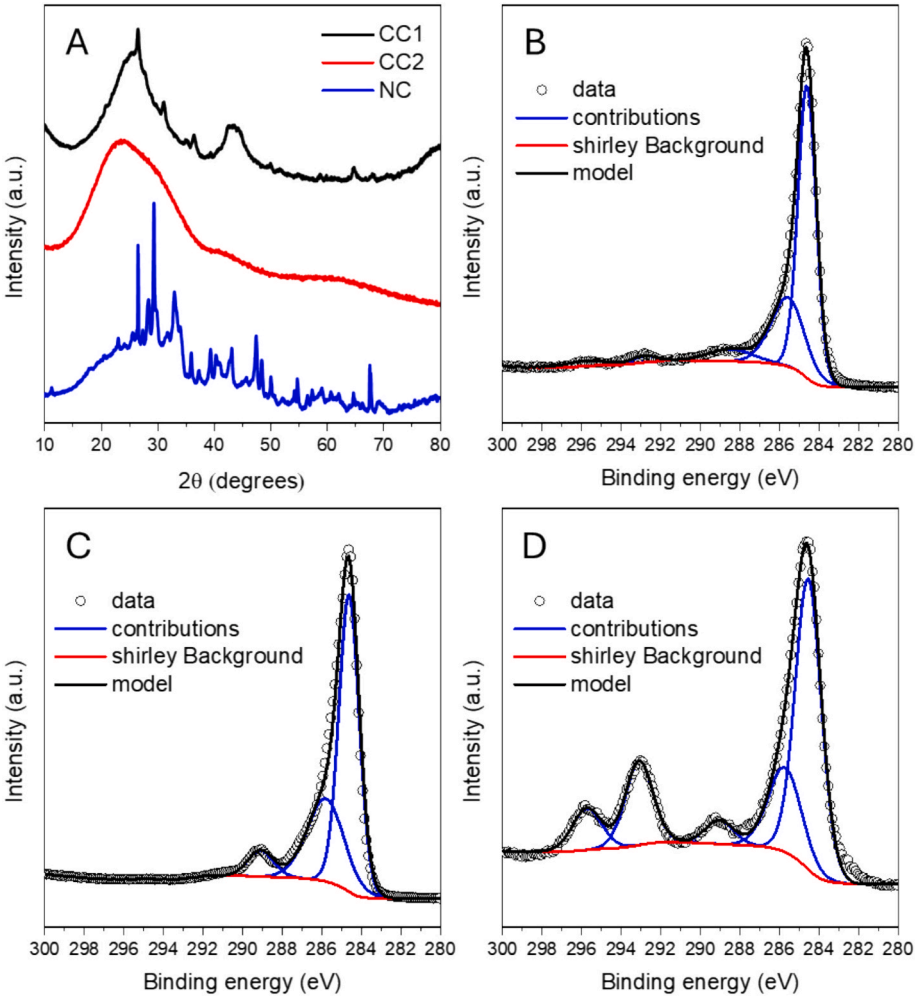

Fig. 1. (A) X-ray diffraction (XRD) patterns of the samples. (B-D) High-resolution XPS C 1s spectra of (B) CC1, (C) CC2, and (D) NC.

2021; Calero et al., 2025). The position and breadth of the (0 0 2)-like band permits a qualitative comparison of the average interlayer spacing (d 0 0 2) and stacking coherence (Jurkiewicz et al., 2018; Sharma et al., 2000). The commercial carbon CC2 shows a very broad maximum centered at 24.6° with only a faint shoulder at 41.8°, which is characteristic of a highly disordered turbostratic carbon with negligible crystalline impurities; the corresponding d 0 0 2 is ≈ 0.361 nm, well above the graphitic value (0.335 nm), corroborating poor layer stacking. For CC1 (carbon from extruded mineral), the broad carbon band around 25° is superimposed on a relatively intense and sharp peak at 26.5°, accompanied by additional reflections at 31.25°, 35.12°, 36.5°, and 64° which can be associated, for example, with quartz or other

impurities, mainly potassium carbonates (Calero et al., 2025; Dehkhoda et al., 2014; Sun et al., 2011), in line with the mineral origin of this carbon. The apparent sharpening near 26.5° suggests a slightly smaller d 0 0 2 (~0.336 nm), although this value is partially biased by the overlapping quartz contribution. The laboratory-made carbon (NC) exhibits the broadest carbon band, centered at ~23° (d 0 0 2 ≈ 0.386 nm), reflecting the highest degree of structural disorder among the three samples. This band overlaps with numerous sharp reflections at 26.5°, 29.4°, 33.18°, 36.01°, 47.5°, and 68°, which can be assigned to a mixture of quartz (SiO_2), calcite ($CaCO_3$), and K-bearing salts (e.g., KCl, K_2CO_3), consistent with the heterogeneous inorganic residue expected from a plastic waste/olive-cake precursor (Chen et al., 2024; Martín-Lara et al., 2021; Zhang et al., 2022).

High-resolution XPS C 1 s spectra (Fig. 1B–D) further elucidate the surface chemical state. All samples exhibit a dominant component at 284.6 eV (sp^2-hybridized C–C) and a second contribution at 285.7 eV (sp^3 C–C or C–O) (Ligero et al., 2024; Zhang et al., 2022). A higher-binding-energy component at 289.0 eV can be assigned to O–C=O species and carbonates, which is particularly relevant in materials that may contain ash. The NC sample (Fig. 1D) shows the most complex envelope, with well-defined peaks at 284.6, 285.7, and 289.0 eV, plus two additional, intense signals at 293.1 and 295.7 eV. These latter peaks do not arise from carbon but coincide with the K $2p_{3/2}$ (~293.2 eV) and K $2p_{1/2}$ (~296.0 eV) doublet, unequivocally evidencing a high surface concentration of potassium (Feng et al., 2020), fully aligned with the multitude of K-containing crystalline phases detected by XRD and the elemental analysis obtained by XPS (K = 5.6 wt%). The strong 289.0 eV contribution, together with the K 2p doublet, indicates a surface enriched in carbonates and potassium salts. In CC1 (Fig. 1B), the same set of components is present, but the high-binding-energy features are markedly weaker, reflecting a lower abundance of surface carbonates and K species, also in line with XPS elemental analysis (K = 1.8 wt%). Finally, CC2 (Fig. 1C) displays only the 284.6, 285.7, and 289.0 eV signals, confirming the minimal presence of inorganic residues and corroborating the featureless nature of its XRD pattern.

Overall, the combined XRD-XPS picture is self-consistent. CC2 is essentially a clean, highly disordered turbostratic carbon with low ash content; CC1 contains moderate quartz and alkali/mineral impurities, evident both in its diffraction pattern and in the weak high-BE XPS features; and NC is a highly disordered carbon matrix heavily loaded with crystalline quartz, calcite, and K/Ca salts, which dominate both its diffraction pattern and its C 1s envelope via the emergence of the K 2p doublet. We note that proper deconvolution of the C 1s region in K-rich samples should explicitly include the K 2p doublet to avoid artificial inflation of high-binding-energy "carbon" contributions. These results highlight the strong interplay between precursor composition/processing and the resulting structural disorder, mineralogy, and surface chemistry of the obtained carbons.

The surface properties of the samples were further evaluated by chemisorption analysis with TPD (Fig. 2). The results revealed significant differences among the commercial materials (CC1, CC2) and the synthesized NC. In the case of CC1, a clear and intense desorption signal was observed at around 670 °C, which can be associated with the presence of stable oxygenated functionalities such as phenolic groups and partially carbonyl-type species (Pereira et al., 2025; Rocha et al., 2023). Conversely, CC2 exhibited a rather featureless profile, characterized by a broad but weak contribution above 850 °C, suggesting a limited amount of strongly bonded oxygenated surface groups.

The synthesized NC displayed a more complex profile, closer to that typically reported for chars derived from biomass (Herold et al., 2022). In particular, NC presented a broad band extending above 700 °C, indicative of carbonyl and quinone-type groups, together with additional contributions at lower temperatures, around 300 and close to 500 °C, which are consistent with the desorption of carboxylic and anhydride functionalities (Pereira et al., 2025; Rocha et al., 2023). The combination of these bands points to heterogeneous surface chemistry,

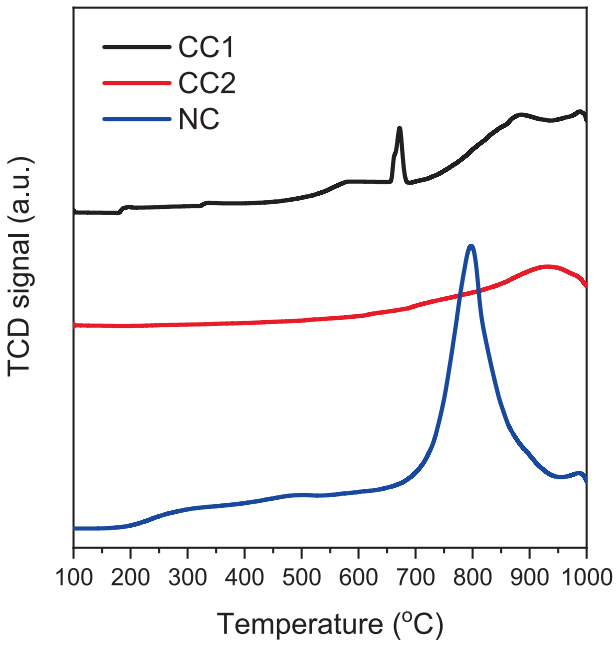

Fig. 2. Chemisorption analysis by TPD of the NC sample and the commercial materials CC1 and CC2.

in agreement with the higher structural diversity of oxygenated groups in the NC sample compared with the commercial references.

3.2. CO_2 adsorption–desorption behavior

3.2.1. CO_2 adsorption

The CO_2 adsorption capacities of the three activated carbon materials, CC1, CC2, and NC, were evaluated under increasing concentrations (20 %, 40 %, and 80 %) and across three adsorption–desorption cycles. The results, displayed in Supplementary Materials (**Fig. S1**) and Fig. 3, demonstrate that CO_2 uptake was positively correlated with the CO_2 feed concentration, as expected due to the increased driving force for adsorption (Li et al., 2017).

Among the three materials, CC2 consistently exhibited the highest adsorption capacities, reaching 2.90 mmol/g (127.61 mg/g) at 80 % CO_2 in cycle 1. This can be attributed to its greater surface area and

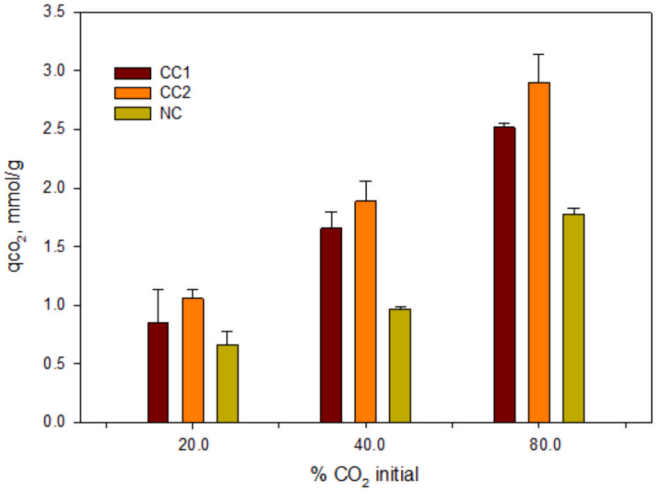

Fig. 3. Comparison of average CO_2 adsorption capacities across cycles 1–3 at different concentrations for each material. Error bars represent the standard deviations between cycles for each material and initial concentration.

microporosity, which are favorable for CO_2 physisorption (Gautam, 2022; Pimentel et al., 2023; Rehman and Park, 2020; Serafin et al., 2022). NC showed the lowest performance across all concentrations, with a maximum of 1.78 mmol/g (78.13 mg/g) at 80 % CO_2 in cycle 1. This limited capacity is likely due to its poorly optimized pore structure, resulting from high structural disorder and substantial inorganic contamination, as revealed by XRD and XPS analyses. The presence of mineral residues likely obstructs micropores and restricts CO_2 access, explaining the reducing adsorption efficiency.

Over the three cycles, minor reductions in adsorption capacity were observed in some cases, particularly for CC1 at 20 % CO_2, where capacity decreased from 1.42 to 1.00 mmol/g from cycle 2 to 3. However, the variations were not systematic and, in some cases, such as CC2, the capacity slightly increased with cycling (e.g., from 1.89 to 2.24 mmol/g at 40 % CO_2), possibly due to the experimental error inherent to the analytical method or to the removal of residual impurities during successive adsorption–desorption cycles, which may improve diffusion pathways (Qasem et al., 2021).

Regarding breakthrough and exhaustion times (data provided in Supplementary Materials), CC2 maintains a constant t_{break} and exhibits high t_{exh} values (often $>$ 133 s), suggesting a slower saturation process and higher adsorption capacity as it was commented before. In contrast, NC presented the worst performance among the three materials, with the lowest t_{break} and t_{exh} values. As CO_2 concentration increases, there is a general trend of slightly decreasing t_{break} and t_{exh}, especially for CC1 and NC materials. Finally, the performance is generally stable across the three adsorption cycles, confirming good repeatability. In other hand, the standard deviations for CO_2 measurements in each cycle ranged between 0.02 and 0.29, further supporting the consistency of the results.

The distinct adsorption performances of CC1, CC2, and NC can be explained by their different adsorption mechanisms. In CC2 sample, the high BET surface area and micropore volume provide abundant adsorption sites for physisorption of CO_2 via van der Waals interactions within narrow pores (Serafin et al., 2022). In addition, the probable presence of nitrogen functionalities, as revealed by elemental analysis, can further enhance CO_2 adsorption through Lewis basic sites. This claim was previously shown in MOFs and doped graphene (Wang et al., 2021; Zhu et al., 2024). For CC1, despite its low surface area (2.82 m^2/g), adsorption probably occurs on external surfaces and at defect sites, while its mineral impurities may contribute to minor chemisorption via carbonate formation. However, adsorption is less efficient than in CC2. In the case of NC, although the developed pore structure is moderate (total: 230.04 m^2/g; micropore: 148.63 m^2/g) and higher than that of CC1 material, the CO_2 adsorption is low and probably limited by the severe structural disorder due to the high content of inorganic residues, which could reduce accessibility to adsorption sites.

The CO_2 adsorption capacities observed in this study (maximum values of 2.90 mmol/g) are reasonably consistent with values reported in the literature for carbons derived from various biomass and polymeric precursors. For instance, activated carbon spheres demonstrated a capacity of 4.55 mmol/g at 25 °C (Wickramaratne and Jaroniec, 2013), while carbon foams with high BET surface areas and significant volumes of narrow micropores (0.59–0.71 cm^3/g) achieved CO_2 uptakes up to 5.0 mmol/g under similar conditions (Cruz et al., 2023). Likewise, adsorption values as high as 5.18 mmol/g at 0 °C and 1 bar have been reported for KOH-activated carbon materials (Kiełbasa et al., 2022), surpassing other high-performance adsorbents such as those with 3.31 mmol/g under identical conditions (Yuan et al., 2022). Additional studies report capacities of 3.44 mmol/g at 25 °C (Dassanayake et al., 2018) and 3.3 mmol/g for $KHCO_3$-activated hydrochar at room temperature (Vega et al., 2024). At lower CO_2 concentrations (e.g., 10–20 %), adsorption capacities generally range from 8 to 34 mg/g (0.18 to 0.77 mmol/g) depending on the porosity and surface chemistry of the activated carbon, with higher feed concentrations (up to 40 % or more) further enhancing uptake performance (Al Mesfer et al., 2021; Ligero et al., 2023).

3.2.2. CO_2 desorption

The CO_2 desorption performance is illustrated in Supplementary Materials (**Fig. S2**) and detailed in Table 2. Desorption performance varies with carbon material type and CO_2 concentration. At low CO_2 concentrations, NC exhibits the highest desorption efficiency (average 96.83 %) despite having the lowest adsorbed amount, while commercial formulas show lower efficiencies (69.25 % and 73.82 %, respectively). At high CO_2 concentrations, all materials show increased desorbed amounts, particularly CC2 (2.55 mmol/g) since a higher amount of CO_2 was adsorbed in the previous adsorption stage, with high efficiency (96.00 %), followed by CC1 (2.17 mmol/g, 88.34 %) and NC (1.45 mmol/g, 84.60 %).

Although NC was the material with a worst adsorption behaviour, its strong regeneration performance highlights the suitability of this material for repeated adsorption–desorption cycles without significant degradation in functionality, being this a key criterion for industrial gas separation applications (Al Atrach et al., 2025).

3.3. CH_4 adsorption–desorption behavior

3.3.1. CH_4 adsorption

CH_4 adsorption was evaluated under the same conditions as CO_2, with results shown in Supplementary Materials (**Fig. S1**) and Fig. 4. Overall, adsorption capacities for CH_4 were significantly lower than for CO_2, which is consistent with data previously reported in literature and it is due to the CH_4's lower quadrupole moment and weaker interactions with the carbon surface(Han et al., 2022; Liu et al., 2023, 2019; Niu et al., 2025; Pancione et al., 2024). For example, for CC2 sample, CO_2 adsorption capacities were two to four times higher than those for CH_4 at the same feed concentration, temperature and pressure. On the other hand, if the performance of the three studied materials is compared, at 80 % CH_4, CC1 reached the highest uptake of 1.43 mmol/g (22.94 mg/g). NC once again showed the lowest capacity, with a maximum of 0.61 mmol/g (9.78 mg/g). Adsorption trends were generally stable across the three cycles, with no significant degradation observed, which confirms the mechanical and structural integrity of the sorbents under CH_4 exposure. The standard deviations for CH_4 measurements in each cycle ranged between 0.01 and 0.04, further supporting the consistency of the results.

3.3.2. CH_4 desorption

CH_4 desorption performance is presented in Supplementary Materials (**Fig. S2**) and Table 3. At low CO_2 concentrations, the three materials show high desorption efficiencies, with CC1 averaging 96.28 %, CC2 91.63 %, and NC 95.26 %. At high CO_2 concentrations, although the desorbed amount increases significantly, the efficiency drops, particularly for CC2 (82.51 %), indicating incomplete desorption at higher loadings. NC maintains nearly 100 % desorption efficiency across all concentrations despite lower overall adsorption.

To better compare the performance of the three carbon materials under varying feed gas concentrations and during three adsorption–desorption cycles, a comprehensive performance index (CPI) was defined and calculated by multiply the following three key parameters, CO_2/CH_4 selectivity (in mg/g), total amount of CO_2 adsorbed in the three cycles, and total recovery efficiency (%). The values are summarized in Table 4. CC2 carbon generally shows the best overall performance, with the highest CPI values at all concentrations. A high value was specially observed at 80 %, reaching a CPI value of 0.52. On the other hand, NC, demonstrated high recovery efficiency but had the lowest CO_2 adsorption capacity, which limits its overall CPI, especially at lower concentrations. However, at high concentrations, its performance can be considered improved.

Table 2
CO_2 desorbed (mmol/g, mg/g) and desorption efficiency (%) at 20%, 40%, and 80% for each cycle and carbon material.

Initial feed concentration	Cycle	CC1			CC2			NC		
		mmol/g	mg/g	%	mmol/g	mg/g	%	mmol/g	mg/g	%
20 %	1	0.87	38.44	87.31	0.92	40.59	83.91	0.61	26.68	91.13
	2	0.68	30.02	48.20	0.81	35.43	74.47	0.47	26.91	99.36
	3	0.72	31.80	72.23	0.76	33.40	63.09	0.48	27.09	100.00
	Average	0.76	33.42	69.25	0.83	36.48	73.82	0.52	26.89	96.83
40 %	1	1.09	48.02	72.73	14.35	63.14	75.97	1.03	45.14	100.00
	2	1.21	53.44	73.22	12.31	54.15	60.28	1.02	44.97	100.00
	3	1.10	48.37	77.56	12.88	56.67	57.60	0.97	42.50	100.00
	Average	1.13	49.94	74.50	1.32	57.99	64.62	1.00	44.20	100.00
80 %	1	2.15	94.60	87.47	2.95	129.65	98.23	1.55	67.99	86.99
	2	2.18	95.99	88.77	2.49	109.64	99.36	1.23	54.05	73.35
	3	2.18	95.99	88.77	2.22	97.82	90.40	1.59	69.75	93.45
	Average	2.17	95.53	88.34	2.55	112.37	96.00	1.45	63.93	84.60

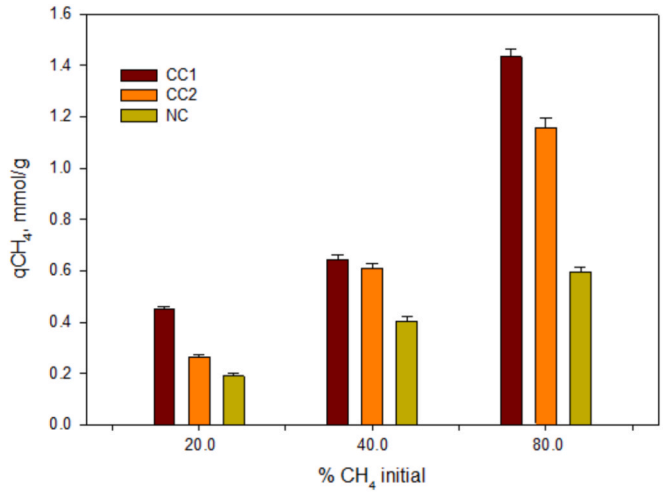

Fig. 4. Comparison of CH_4 adsorption capacities across cycles 1–3 at different concentrations for each material. Error bars represent the standard deviations between cycles for each material and initial concentration.

3.4. *Comparison of the activated carbons in a real application (upgrading of biogas)*

To simulate a realistic gas separation scenario, the three materials were tested with a synthetic biogas mixture (45 % CO_2, 55 % CH_4) in three consecutive adsorption–desorption cycles. The corresponding adsorption and desorption profiles are shown in Supplementary Materials (**Fig. S3**), and the quantitative results are summarized in Table 5.

Under these conditions, CC2 displayed the highest CO_2 uptake (1.41 mmol/g, 61.94 mg/g), while maintaining moderate CH_4 uptake (0.59 mmol/g, 9.74 mg/g). This led to the highest CO_2/CH_4 selectivity (2.40 in molar terms and 6.36 in mass terms), indicating its potential for biogas upgrading applications.

However, the NC material, developed from a blend of plastic and olive pomace, exhibited lower CO_2 uptake (0.80 mmol/g) and a higher CH_4 adsorption (0.93 mmol/g), resulting in lower CO_2/CH_4 selectivity of 0.86. This behavior can be attributed to the limited presence of oxygen-containing surface groups, which usually enhance the affinity toward CO_2 through specific interactions (Song et al., 2020), together with the high inorganic content that can block pores and reduce accessible sites and moderate porosity development. To overcome this drawback, targeted modifications such as surface functionalization to introduce nitrogen- or oxygen-containing groups (Quan et al., 2023; Shao et al., 2024), chemical activation to develop a microporous framework with higher surface area (Kamran and Park, 2021) and acid-washing to remove mineral matter and avoid pore blockage (Gęsikiewicz-Puchalska et al., 2017) have been effective for improving CO_2 adsorption and CO_2/CH_4 selectivity in carbon materials. For instance, N-doped waste-derived carbons achieved CO_2/CH_4 selectivities above 3.2 at ambient conditions (Li et al., 2019), while commercial coconut-shell activated carbon reached values of 4.7 at 1 bar and 298 K (Staudt et al., 2024). Even higher selectivities, between 1.8 and 9.1, have been reported for cashew nut shell carbons activated with K_2CO_3

Table 3
CH_4 desorbed (mmol/g, mg/g) and desorption efficiency (%) at 20%, 40%, and 80% for each cycle and carbon material.

Initial feed concentration	Cycle	CC1			CC2			NC		
		mmol/g	mg/g	%	mmol/g	mg/g	%	mmol/g	mg/g	%
20 %	1	0.45	7.11	99.33	0.30	8.05	100.00	0.20	3.26	100.00
	2	0.40	7.35	89.50	0.27	7.77	100.00	0.16	4.25	85.78
	3	0.44	7.59	100.00	0.19	7.77	74.90	0.19	4.10	100.00
	Average	0.43	7.35	96.28	0.25	7.86	91.63	0.19	3.87	95.26
40 %	1	0.66	15.29	99.24	0.65	10.40	99.54	0.40	6.34	98.02
	2	0.56	8.97	89.90	0.59	9.49	90.81	0.41	6.50	95.53
	3	0.62	9.97	94.25	0.54	8.60	82.39	0.41	7.47	100.00
	Average	0.61	11.41	94.46	0.59	9.50	90.91	0.40	6.77	97.85
80 %	1	1.37	21.92	95.54	1.25	20.05	100.00	0.65	10.37	100.00
	2	1.43	22.80	100.00	0.96	15.38	81.58	0.58	9.34	100.00
	3	1.07	17.06	77.47	0.73	11.62	65.94	0.61	9.76	99.84
	Average	1.29	20.59	91.00	0.98	15.68	82.51	0.61	9.82	99.95

Table 4
Performance indicators for CO_2/CH_4 separation by CC1, CC2, and NC at different feed concentrations (20%, 40%, and 80%).

Material	Initial feed concentration, %	Selectivity$_{mg/g}$	Normalized selectivity*	Total CO_2 adsorption, mg/g	Normalized adsorption*	Total recovery efficiency, %	Normalized recovery*	CPI
CC1	20	6.72	0.56	143.58	0.41	87.3	0.86	0.20
	40	6.76	0.56	208.08	0.60	72.7	0.72	0.24
	80	7.83	0.65	327.06	0.94	85.3	0.84	0.51
CC2	20	12.07	1.00	151.41	0.44	83.9	0.83	0.36
	40	8.75	0.72	271.33	0.78	76.0	0.75	0.43
	80	6.30	0.52	346.15	1.00	101.6	1.00	0.52
NC	20	7.84	0.65	70.84	0.20	91.1	0.90	0.12
	40	6.50	0.54	125.99	0.36	100.0	0.98	0.19
	80	7.96	0.66	226.40	0.65	87.0	0.86	0.37

* Normalized values were obtained by dividing each raw parameter (selectivity, CO_2 adsorption, and recovery efficiency) by the highest value observed among all materials. This allows direct comparison of relative performance across different metrics.

Table 5
Adsorption and desorption capacities (mmol/g, mg/g) of CO_2 and CH_4 from synthetic biogas for each material.

Cycle	Parameter		CC1			CC2			NC		
			mmol/g	mg/g	Efficiency, %	mmol/g	mg/g	Efficiency, %	mmol/g	mg/g	Efficiency, %
1	**qCO_2**	Adsorption	0.95	41.78	100	1.41	61.94	92	0.80	35.00	103
	qCO_2	Desorption	0.95	41.96		1.29	56.92		0.82	36,09	
	qCH_4	Adsorption	0.92	14.67	95	0.59	9.74	100	0.93	14.79	98
	qCH_4	Desorption	0.87	13.97		0.59	9.74		0.91	14.64	
	Selectivity CO_2/CH_4	Adsorption	1.04	2.85	–	2.40	6.36	–	0.86	2.37	–
2	**qCO_2**	Adsorption	0.86	37.70	106	1.23	54.16	109	0.70	30.64	111
	qCO_2	Desorption	0.91	40.04		1.34	58.96		0.77	33.88	
	qCH_4	Adsorption	0.98	15.92	91	0.57	9.12	105	0.88	14.07	101
	qCH_4	Desorption	0.90	14.48		0.60	9,61		0.89	14.22	
	Selectivity CO_2/CH_4	Adsorption	0.88	2.37	–	2.16	5.94	–	0.80	2.18	–
3	**qCO_2**	Adsorption	0.89	39.09	102	1.33	58.40	102	0.72	31.68	104
	qCO_2	Desorption	0.91	40.04		1.35	59.31		0.75	33.01	
	qCH_4	Adsorption	0.95	15.29	97	0.65	10.53	101	0.90	14.52	92
	qCH_4	Desorption	0.92	14.78		0.66	10.66		0.83	13.34	
	Selectivity CO_2/CH_4	Adsorption	0.94	2.56	–	2.05	5.55	–	0.80	2.18	–

(Fonseca-Bermúdez et al., 2024). Compared to these benchmarks, the current NC selectivity is low, but its waste-derived origin provides significant opportunities for optimization through targeted post-treatments.

The TPD analysis provides valuable insight into the distinct CO_2/CH_4 separation behaviours observed across the series. CC1 exhibits a pronounced desorption event at ca. 670 °C, indicative of a relatively high density of stable oxygenated acidic moieties (phenolic/partial carbonyl), which typically lowers the effective basicity of edge sites and may partially block ultramicropores, thereby penalizing CO_2 uptake and regeneration. By contrast, the featureless and weak profile of CC2, confined to a broad contribution above 850 °C, reveals a low concentration of oxygenated surface groups consistent with a more graphitic/basic character. Combined with its extensive microporosity, this surface chemistry explains the superior CO_2 capacity and CO_2/CH_4 selectivity measured for CC2, confirming its suitability for biogas upgrading. The NC sample, obtained from plastic/olive-cake co-pyrolysis, displays a heterogeneous surface (bands > 700 °C plus contributions at ~300 and ~500 °C) akin to biomass-derived chars, which, together with its lower surface area, translates into a reduced CO_2 capacity.

On the other hand, CC1 showed an intermediate behavior, with similar CO_2 and CH_4 uptakes (0.95 and 0.92 mmol/g, respectively), and a modest selectivity (1.04).

In terms of regenerability, all materials showed good desorption performance over three cycles, with high desorption yields maintained (indicating nearly complete desorption and, in some cases, apparent over-desorption likely related to experimental variability). In this sense, for CO_2, desorption efficiencies ranged from 100–106 % for CC1, 92–109 % for CC2, and 103–111 % for NC. CC2 and NC materials demonstrated very good regenerability behaviour. Interestingly, while CC2 combined high CO_2 uptake with stable cycling, the NC material also demonstrated excellent regeneration stability despite its lower selectivity. This rapid and nearly complete desorption behavior suggests that NC has a relatively weak interaction with CO_2, which, although detrimental for separation efficiency, can be advantageous for cyclic operation where easy regeneration and reduced energy demand are key factors. In this context, pelletization of NC is recommended to improve processability in practical fixed-bed operations.CH_4 desorption was similarly efficient, with recoveries between 91–97 % for CC1, 100–105 % for CC2, and 92–101 % for NC, further supporting the excellent regenerability of these sorbents.

4. Conclusions

Characterization and performance data indicate that CC2 combines high carbon content, extensive microporosity and the best CO_2 adsorption/selectivity among the tested materials, confirming its suitability for biogas upgrading. NC, prepared from plastic/olive-cake co-pyrolysis, shows a markedly lower BET area and CO_2 capacity but displays near-complete desorption and excellent regeneration stability over repeated cycles. The XRD/XPS and proximate analyses also reveal high ash and potassium/calcium salt content in NC, which partially explains its

limited micropore development and current low selectivity.

Despite inferior uptake and selectivity relative to CC2, NC's robust regenerability, low production cost and valorization of abundant wastes make it a promising platform for a cost-effective, environmentally friendly cyclic adsorbent.

To enhance NC's competitiveness, a focused modification pathway was recommended: i) demineralization by acid washing, e.g., dilute HCl to remove surface salts/ash (K, Ca, carbonates) detected by XRD/XPS to reduce inorganic blockage; ii) optimized activation to increase microporosity, for example, exploring chemical activation strategies; iii) functionalization introducing nitrogen- or oxygen-containing groups by specific treatments like urea impregnation; iv) pelletization to improve processability for cycles in fixed-bed columns..

Declaration of Generative AI and AI-assisted technologies in the writing process

During the preparation of this work, the authors used ChatGPT to improve the writing style and the fluency of the English language. After using this tool/service, the authors reviewed and edited the content as needed and took full responsibility for the content of the published article.

CRediT authorship contribution statement

María Ángeles Martín-Lara: Writing – review & editing, Writing – original draft, Supervision, Project administration, Funding acquisition, Formal analysis, Data curation. **Mario J. Muñoz-Batista:** Writing – review & editing, Writing – original draft, Visualization, Software, Formal analysis. **Gabriel Blázquez:** Validation, Supervision, Resources, Methodology, Investigation. **Ledicia Pereira:** Writing – original draft, Validation, Investigation. **Alejandra Quintana:** Writing – original draft, Methodology, Investigation. **Mónica Calero:** Writing – review & editing, Supervision, Software, Project administration, Funding acquisition, Formal analysis, Data curation, Conceptualization.

Declaration of competing interest

The authors declare that they have no known competing financial interests or personal relationships that could have appeared to influence the work reported in this paper.

Acknowledgments

Project PDC2022-133808-I00 (ADSORCHAR) was financed by MICIU/AEI /10.13039/501100011033 and the European Union Next Generation EU/ PRTR. The authors are also grateful to the external analysis services CIC ("Centro de Instrumentación Científica") of the University of Granada.

Appendix A. Supplementary material

Supplementary data to this article can be found online at https://doi.org/10.1016/j.wasman.2025.115223.

Data availability

No data was used for the research described in the article.

References

Aissaoui, M.H., Trabelsi, A.B.H., bensidhom, G., Ceylan, S., Leahy, J.J., Kwapinski, W., 2023. Insights into olive pomace pyrolysis conversion to biofuels and biochars: Characterization and techno-economic evaluation. Sustain Chem Pharm 32, 101022. Doi: 10.1016/j.scp.2023.101022.

Akhtar, M.S., Ali, S., Zaman, W., 2024. Innovative adsorbents for pollutant removal: exploring the latest research and applications. Molecules 29, 4317. https://doi.org/10.3390/molecules29184317.

Al Atrach, J., Aitblal, A., Amedlous, A., Clatworthy, E.B., Honorato Piva, D., Xiong, Y., Guillet-Nicolas, R., Valtchev, V., 2025. Exploring a novel adsorbent for CO_2 capture and gas separation. ACS Appl. Mater. Interfaces 17, 7119–7130. https://doi.org/10.1021/acsami.4c18745.

Al Mesfer, M.K., Amari, A., Danish, M., Al Alwan, B.A., Shah, M., 2021. Simulation study of fixed-bed CO_2 adsorption from CO_2 /N_2 mixture using activated carbon. Chem. Eng. Commun. 208, 1358–1367. https://doi.org/10.1080/00986445.2020.1777111.

Angelidaki, I., Treu, L., Tsapekos, P., Luo, G., Campanaro, S., Wenzel, H., Kougias, P.G., 2018. Biogas upgrading and utilization: current status and perspectives. Biotechnol. Adv. 36, 452–466. https://doi.org/10.1016/j.biotechadv.2018.01.011.

Ashokkumar, V., Kumar, G., Lakshmanan, H., Chandramughi, V.P., Flora, G., Kothari, R., Piechota, G., 2025. A critical review of biogas production and upgrading from organic wastes: recent advances, challenges and opportunities. Biomass Bioenergy 194, 107566. https://doi.org/10.1016/j.biombioe.2024.107566.

Augelletti, R., Conti, M., Annesini, M.C., 2017. Pressure swing adsorption for biogas upgrading. A new process configuration for the separation of biomethane and carbon dioxide. J. Clean. Prod. 140, 1390–1398. https://doi.org/10.1016/j.jclepro.2016.10.013.

Batuecas, E., Tommasi, T., Battista, F., Negro, V., Sonetti, G., Viotti, P., Fino, D., Mancini, G., 2019. Life cycle assessment of waste disposal from olive oil production: anaerobic digestion and conventional disposal on soil. J. Environ. Manage. 237, 94–102. https://doi.org/10.1016/j.jenvman.2019.02.021.

Besinella, G.B., Padilha, J.E., Scheufele, F.B., Gasparrini, L.J., Borba, C.E., Alves, H.J., 2021. Green synthesis of templated carbon porous materials from simple raw materials. Mater. Adv. 2, 403–412. https://doi.org/10.1039/D0MA00483A.

Biniak, S., Szymański, G., Siedlewski, J., Świątkowski, A., 1997. The characterization of activated carbons with oxygen and nitrogen surface groups. Carbon N Y 35, 1799–1810. https://doi.org/10.1016/S0008-6223(97)00096-1.

Boules, A., Tabu, B., Brack, E., Alexander, T., Mack, J.H., Trelles, J.P., 2024. Hydrogen production synergy in non-thermal plasma copyrolysis of low-density polyethylene and cellulose. Int. J. Hydrogen Energy 65, 375–380. https://doi.org/10.1016/j.ijhydene.2024.04.005.

Bukhari, I., Haq, F., Kiran, M., Aziz, T., Mehmood, S., Haroon, M., 2025. Lignocellulosic biomass as a renewable resource: driving second-generation biofuel innovation from agricultural waste. Biomass Bioenergy 201, 108133. https://doi.org/10.1016/j.biombioe.2025.108133.

Calero, M., Blázquez, G., Solís, R.R., Martín-Lara, M.Á., Muñoz-Batista, M.J., 2025. Exploring pyrolysis-based alternatives for the valorization of used diapers through a comprehensive understanding of all generated products. Chem. Eng. J. 503, 158244. https://doi.org/10.1016/j.cej.2024.158244.

Chen, H., Rocha, L.A.O., Zhang, H., Xiong, Y., Zhang, S., 2025. Evaluation of char properties from co-pyrolysis of biomass/plastics: effect of different types of plastics. Process Saf. Environ. Prot. 193, 228–238. https://doi.org/10.1016/j.psep.2024.11.009.

Chen, H., Wang, J., Rocha, L.A.O., Zhang, H., Zhang, S., Zhang, H., 2024. Insights into the char-production mechanism during co-pyrolysis of biomass and plastic wastes. Energy 312, 133642. https://doi.org/10.1016/j.energy.2024.133642.

Cruz, O.F., Gómez, I.C., Rodríguez-Reinoso, F., Silvestre-Albero, J., Rambo, C.R., Martínez-Escandell, M., 2023. Activated carbons with high micropore volume obtained from polyurethane foams for enhanced CO_2 adsorption. Chem. Eng. Sci. 273, 118671. https://doi.org/10.1016/j.ces.2023.118671.

Cupertino, G.F.M., da Silva, Á.M., Pereira, A.K.S., Delatorre, F.M., Ucella-Filho, J.G.M., de Souza, E.C., Profeti, D., Profeti, L.P.R., Oliveira, M.P., Saloni, D., Luque, R., Dias Júnior, A.F., 2024. Co-pyrolysis of biomass and polyethylene terephthalate (PET) as an alternative for energy production from waste valorization. Fuel 362, 130761. https://doi.org/10.1016/j.fuel.2023.130761.

Dan, E., McCue, A.J., Dionisi, D., Fernández Martín, C., 2024. Household mixed plastic waste derived adsorbents for CO_2 capture: a feasibility study. J. Environ. Manage. 355, 120466. https://doi.org/10.1016/j.jenvman.2024.120466.

Dassanayake, R.S., Gunathilake, C., Abidi, N., Jaroniec, M., 2018. Activated carbon derived from chitin aerogels: preparation and CO_2 adsorption. Cellul. 25, 1911–1920. https://doi.org/10.1007/s10570-018-1660-3.

Dehkhoda, A.M., Ellis, N., Gyenge, E., 2014. Electrosorption on activated biochar: effect of thermo-chemical activation treatment on the electric double layer capacitance. J. Appl. Electrochem. 44, 141–157. https://doi.org/10.1007/s10800-013-0616-4.

Deng, J., Yi, B., Mašek, O., Yuan, X., Hwang, S.Y., Ong, H.C., Hua, Z., Ok, Y.S., 2025. Co-pyrolysis of biomass and plastic waste into carbon materials with environmental applications: a critical review. Green Chem. 27, 6320–6341. https://doi.org/10.1039/D4GC04842C.

Feng, W., Cui, Y., Liu, W., Wang, H., Zhang, Y., Du, Y., Liu, S., Wang, H., Gao, X., Wang, T., 2020. Rigid-flexible coupling carbon skeleton and potassium-carbonate-dominated solid electrolyte interface achieving superior potassium-ion storage. ACS Nano 14, 4938–4949. https://doi.org/10.1021/acsnano.0c01073.

Ferreira, C.I.A., Calisto, V., Cuerda-Correa, E.M., Otero, M., Nadais, H., Esteves, V.I., 2016. Comparative valorisation of agricultural and industrial biowastes by combustion and pyrolysis. Bioresour. Technol. 218, 918–925. https://doi.org/10.1016/j.biortech.2016.07.047.

Fonseca-Bermúdez, Ó.J., Giraldo, L., Sierra-Ramírez, R., Serafin, J., Dziejarski, B., Bonillo, M.G., Farid, G., Moreno-Piraján, J.C., 2024. Cashew nut shell biomass: a source for high-performance CO_2/CH_4 adsorption in activated carbon. J. CO2 Util. 83, 102799. https://doi.org/10.1016/j.jcou.2024.102799.

Gautam, S.S., 2022. Experimental investigation on different activated carbons as adsorbents for CO_2 capture. Therm. Sci. Eng. Prog. 33, 101339. https://doi.org/10.1016/j.tsep.2022.101339.
Gęsikiewicz-Puchalska, A., Zgrzebnicki, M., Michalkiewicz, B., Narkiewicz, U., Morawski, A.W., Wrobel, R.J., 2017. Improvement of CO_2 uptake of activated carbons by treatment with mineral acids. Chem. Eng. J. 309, 159–171. https://doi.org/10.1016/j.cej.2016.10.005.
Gimenez, M., Rodríguez, M., Montoro, L., Sardella, F., Rodríguez-Gutierrez, G., Monetta, P., Deiana, C., 2020. Two phase olive mill waste valorization. Hydrochar production and phenols extraction by hydrothermal carbonization. Biomass Bioenergy 143, 105875. https://doi.org/10.1016/j.biombioe.2020.105875.
Guo, S., Li, Y., Wang, Y., Wang, L., Sun, Y., Liu, L., 2022. Recent advances in biochar-based adsorbents for CO_2 capture. Carbon Capture Sci. Technol. 4, 100059. https://doi.org/10.1016/j.ccst.2022.100059.
Han, S.-J., Sang, S.-X., Duan, P.-P., Zhang, J.-C., Xiang, W.-X., Xu, A., 2022. The effect of the density difference between supercritical CO_2 and supercritical CH_4 on their adsorption capacities: an experimental study on anthracite in the Qinshui Basin. Pet. Sci. 19, 1516–1526. https://doi.org/10.1016/j.petsci.2022.03.003.
Herold, F., Gläsel, J., Etzold, B.J.M., Rønning, M., 2022. Can temperature-programmed techniques provide the gold standard for carbon surface characterization? Chem. Mater. 34, 8490–8516. https://doi.org/10.1021/acs.chemmater.2c02449.
Hongthong, S., Sangsida, W., Wongcharee, S., Chanthakhot, A., Aungthitipan, P., Suwannahong, K., Kreetachat, T., Rioyo, J., 2024. Enhanced biochar production via co-pyrolysis of biomass residual with plastic waste after recycling process. Int. J. Chem. Eng. 2024. https://doi.org/10.1155/2024/1176275.
Hu, H., Guo, X., Yang, L., Wu, Y., Yang, G., Luo, X., 2025a. Adsorption materials toward highly-efficient lithium extraction from non-conventional lithium sources. Adv. Mater. 37. https://doi.org/10.1002/adma.202506055.
Hu, H., Yang, G., Chen, C., Guo, X., Xie, Y., Hou, D., Li, X., Fan, W., Yang, L., Luo, X., 2025b. Ultra−selective and capacious lithium extraction from geothermal brines via β −diketone functionalized brush−shaped polymer. Adv. Funct. Mater. https://doi.org/10.1002/adfm.202513012.
Hulicova-Jurcakova, D., Seredych, M., Lu, G.Q., Bandosz, T.J., 2009. Combined effect of nitrogen- and oxygen-containing functional groups of microporous activated carbon on its electrochemical performance in supercapacitors. Adv. Funct. Mater. 19, 438–447. https://doi.org/10.1002/adfm.200801236.
Jansen, R.J.J., van Bekkum, H., 1995. XPS of nitrogen-containing functional groups on activated carbon. Carbon N Y 33, 1021–1027. https://doi.org/10.1016/0008-6223(95)00030-H.
Jurkiewicz, K., Pawlyta, M., Burian, A., 2018. Structure of carbon materials explored by local transmission electron microscopy and global powder diffraction probes. C (Basel) 4, 68. https://doi.org/10.3390/c4040068.
Jurkiewicz, M., Musik, M., Pełech, R., 2023. Adsorption of a four-component mixture of volatile organic compound vapors on modified activated carbons. Ind. Eng. Chem. Res. 62, 3716–3723. https://doi.org/10.1021/acs.iecr.2c04572.
Kamran, U., Park, S.-J., 2021. Chemically modified carbonaceous adsorbents for enhanced CO_2 capture: a review. J. Clean. Prod. 290, 125776. https://doi.org/10.1016/j.jclepro.2020.125776.
Kiełbasa, K., Bayar, Ş., Varol, E.A., Sreńscek-Nazzal, J., Bosacka, M., Miądlicki, P., Serafin, J., Wróbel, R.J., Michalkiewicz, B., 2022. Carbon dioxide adsorption over activated carbons produced from molasses using H_2SO_4, H_3PO_4, HCl, NaOH, and KOH as activating agents. Molecules 27, 7467. https://doi.org/10.3390/molecules27217467.
Kumar, M., Seth, A., Singh, A.K., Rajput, M.S., Sikandar, M., 2021. Remediation strategies for heavy metals contaminated ecosystem: a review. Environ. Sustain. Indic. 12, 100155. https://doi.org/10.1016/j.indic.2021.100155.
Lee, T., Kwon, D., Lee, S., Kim, Y., Kim, J.Y., Song, H., Jung, S., Lee, J., Tsang, Y.F., Kim, K.-H., Kwon, E.E., 2025. Recovery of chemicals and energy through thermo-chemical processing of plastic waste. Prog. Energy Combust. Sci. 108, 101219. https://doi.org/10.1016/j.pecs.2025.101219.
Li, X., Zhu, L., Xue, Q., Chang, X., Ling, C., Xing, W., 2017. Superior selective CO_2 adsorption of C_3N pores: GCMC and DFT simulations. ACS Appl. Mater. Interfaces 9, 31161–31169. https://doi.org/10.1021/acsami.7b09648.
Li, Y., Xu, R., Wang, B., Wei, J., Wang, L., Shen, M., Yang, J., 2019. Enhanced N-doped porous carbon derived from KOH-activated waste wool: a promising material for selective adsorption of CO_2/CH_4 and CH_4/N_2. Nanomaterials 9, 266. https://doi.org/10.3390/nano9020266.
Ligero, A., Calero, M., Martín-Lara, M.Á., Blázquez, G., Solís, R.R., Pérez, A., 2023. Fixed-bed CO_2 adsorption onto activated char from the pyrolysis of a non-recyclable plastic mixture from real urban residues. J. CO2 Util. 73, 102517. https://doi.org/10.1016/j.jcou.2023.102517.
Ligero, A., Solís, R.R., Blázquez, G., Muñoz-Batista, M.J., Pérez, A., Calero, M., 2024. On the cutting-edge of non-recyclable plastic waste valorization: from pyrolysis char to nitrogen-enriched activated carbon for landfill biogas upgrading. J. Environ. Chem. Eng. 12, 112265. https://doi.org/10.1016/j.jece.2024.112265.
Liu, B., Wen, H., Cheng, X., Fan, S., Mi, W., Li, R., 2023. Competitive adsorption law of multi-component gases during CO_2 displacement of CH_4 in coal seams. J. CO2 Util. 76, 102581. https://doi.org/10.1016/j.jcou.2023.102581.
Liu, J., Xie, L., Elsworth, D., Gan, Q., 2019. CO_2/CH_4 competitive adsorption in shale: implications for enhancement in gas production and reduction in carbon emissions. Environ. Sci. Technol. 53, 9328–9336. https://doi.org/10.1021/acs.est.9b02432.
Martín-Lara, M.A., Piñar, A., Ligero, A., Blázquez, G., Calero, M., 2021. Characterization and use of char produced from pyrolysis of post-consumer mixed plastic waste. Water (Basel) 13, 1188. https://doi.org/10.3390/w13091188.
Mechnou, I., Mourtah, I., Raji, Y., Chérif, A., Lebrun, L., Hlaibi, M., 2021. Effective treatment and the valorization of solid and liquid toxic discharges from olive oil industries, for sustainable and clean production of bio-coal. J. Clean. Prod. 288, 125649. https://doi.org/10.1016/j.jclepro.2020.125649.
Miao, Y., Qian, Z., Cao, H., Yang, Y., Li, P., 2025. Modelling and experiment for simultaneous biogas upgrading and CO_2 capture by an advanced VPSA-SMB process. Chem. Eng. Sci. 307, 121371. https://doi.org/10.1016/j.ces.2025.121371.
Niu, Y., Wang, Y., Xiong, Y., Wang, Z., Li, L., Zhang, S., Zhai, Z., 2025. Molecular simulation elucidation of gas adsorption and desorption mechanisms in coal micropores: synergistic effects of pore size and CO_2 injection on CH_4 recovery. Langmuir 41, 7570–7579. https://doi.org/10.1021/acs.langmuir.4c05142.
Oñate, A., Travieso Pedroso, D., Valenzuela, M., Blanco Machin, E., Tuninetti, V., 2024. Production of high-calorific hybrid biofuel pellets from urban plastic waste and agro-industrial by-products. J. Clean. Prod. 479, 144046. https://doi.org/10.1016/j.jclepro.2024.144046.
Pancione, E., La Motta, F., Boffa, A., Lancia, A., Erto, A., 2024. Uncovering the potential of MSC CT-350 for CO_2/CH_4 separation toward the optimization of a pressure swing adsorption process for biogas upgrading. Fuel Process. Technol. 256, 108065. https://doi.org/10.1016/j.fuproc.2024.108065.
Patil, V., Adhikari, S., Cross, P., 2018. Co-pyrolysis of lignin and plastics using red clay as catalyst in a micro-pyrolyzer. Bioresour. Technol. 270, 311–319. https://doi.org/10.1016/j.biortech.2018.09.034.
Peredo-Mancilla, D., Ghouma, I., Hort, C., Ghimbeu, C.M., Jeguirim, M., Bessieres, D., 2018. CO_2 and CH_4 adsorption behavior of biomass-based activated carbons. Energies (Basel) 11, 3136. https://doi.org/10.3390/en11113136.
Pereira, L., Calero, M., Blázquez, G., González-Egido, S., González-Lucas, M., Martín-Lara, M.Á., Solís, R.R., 2025. On the physical activation of biomass and urban waste chars for water treatment and CO_2 adsorption. Chem. Eng. Sci. 313, 121749. https://doi.org/10.1016/j.ces.2025.121749.
Pereira, L., Castillo, V., Calero, M., González-Egido, S., Martín-Lara, M.Á., Solís, R.R., 2024. Promoting the circular economy: valorization of a residue from industrial char to activated carbon with potential environmental applications as adsorbents. J. Environ. Manage. 356, 120753. https://doi.org/10.1016/j.jenvman.2024.120753.
Pérez-Huertas, S., Calero, M., Ligero, A., Pérez, A., Terpiłowski, K., Martín-Lara, M.A., 2023. On the use of plastic precursors for preparation of activated carbons and their evaluation in CO_2 capture for biogas upgrading: a review. Waste Manag. https://doi.org/10.1016/j.wasman.2023.02.022.
Pimentel, C.H., Díaz-Fernández, L., Gómez-Díaz, D., Freire, M.S., González-Álvarez, J., 2023. Separation of CO_2 using biochar and KOH and $ZnCl_2$ activated carbons derived from pine sawdust. J. Environ. Chem. Eng. 11, 111378. https://doi.org/10.1016/j.jece.2023.111378.
Plastics Europe, 2024. Plastics - the fast Facts 2024 [WWW Document]. URL https://plasticseurope.org/knowledge-hub/plastics-the-fast-facts-2024/ (accessed 11.3.25).
Pui, W.K., Yusoff, R., Aroua, M.K., 2019. A review on activated carbon adsorption for volatile organic compounds (VOCs). Rev. Chem. Eng. 35, 649–668. https://doi.org/10.1515/revce-2017-0057.
Qasem, N.A.A., Abuelyamen, A., Ben-Mansour, R., 2021. Enhancing CO_2 adsorption capacity and cycling stability of Mg-MOF-74. Arab. J. Sci. Eng. 46, 6219–6228. https://doi.org/10.1007/s13369-020-04946-0.
Quan, C., Zhou, Y., Wang, J., Wu, C., Gao, N., 2023. Biomass-based carbon materials for CO_2 capture: a review. J. CO2 Util. 68, 102373. https://doi.org/10.1016/j.jcou.2022.102373.
Rehman, A., Park, S.-J., 2020. From chitosan to urea-modified carbons: tailoring the ultra-microporosity for enhanced CO_2 adsorption. Carbon N Y 159, 625–637. https://doi.org/10.1016/j.carbon.2019.12.068.
Rocha, R.P., Pereira, M.F.R., Figueiredo, J.L., 2023. Characterisation of the surface chemistry of carbon materials by temperature-programmed desorption: an assessment. Catal. Today 418, 114136. https://doi.org/10.1016/j.cattod.2023.114136.
Sádovská, G., Honcová, P., Morávková, J., Jirka, I., Vorokhta, M., Pilař, R., Rathouský, J., Kaucký, D., Mikysková, E., Sazama, P., 2023. The thermal stability of carbon materials in the air: quantitative structural investigation of thermal stability of carbon materials in air. Carbon N Y 206, 211–225. https://doi.org/10.1016/j.carbon.2023.02.042.
Seah, C.C., Tan, C.H., Arifin, N.A., Hafriz, R.S.R.M., Salmiaton, A., Nomanbhay, S., Shamsuddin, A.H., 2023. Co-pyrolysis of biomass and plastic: circularity of wastes and comprehensive review of synergistic mechanism. Results Eng. 17, 100989. https://doi.org/10.1016/j.rineng.2023.100989.
Serafin, J., Kiełbasa, K., Michalkiewicz, B., 2022. The new tailored nanoporous carbons from the common polypody (polypodium vulgare): the role of textural properties for enhanced CO_2 adsorption. Chem. Eng. J. 429, 131751. https://doi.org/10.1016/j.cej.2021.131751.
Shao, J., Wang, J., Yu, Q., Yang, F., Demir, M., Altinci, O.C., Umay, A., Wang, L., Hu, X., 2024. Unlocking the potential of N-doped porous carbon: facile synthesis and superior CO_2 adsorption performance. Sep. Purif. Technol. 333, 125891. https://doi.org/10.1016/j.seppur.2023.125891.
Sharma, A., Kyotani, T., Tomita, A., 2000. Comparison of structural parameters of PF carbon from XRD and HRTEM techniques. Carbon N Y 38, 1977–1984. https://doi.org/10.1016/S0008-6223(00)00045-2.
Sidabutar, R., Trisakti, B., Irvan, Michael, M., Vanness, V., Alexander, V., Natasya, Y., Pasaribu, D.S.K., Alamsyah, V., Zaiyat, M.Z.Z., Syafriandy, S., Fath, M.T. Al, Dalimunthe, N.F., Abdul, P.M., Takriff, M.S., 2025. Synergistic integration of zeolite engineering and fixed-bed column design for enhanced biogas upgrading: adsorbent synthesis, CO_2/CH_4 separation kinetics, and regeneration assessment. Sep Purif Technol 355, 129772. Doi: 10.1016/j.seppur.2024.129772.
Song, X., Wang, L., Gong, J., Zhan, X., Zeng, Y., 2020. Exploring a new method to study the effects of surface functional groups on adsorption of CO_2 and CH_4 on activated carbons. Langmuir 36, 3862–3870. https://doi.org/10.1021/acs.langmuir.9b03475.

Staudt, J., Musial, C.M., Canevesi, R., Fierro, V., Ribeiro, C., Alves, H.J., Borba, C.E., 2024. Evaluation of the CH_4/CO_2 separation by adsorption on coconut shell activated carbon: Impact of the gas moisture on equilibrium selectivity and adsorption capacity. Heliyon 10, e30368. https://doi.org/10.1016/j.heliyon.2024.e30368.

Sun, K., Ro, K., Guo, M., Novak, J., Mashayekhi, H., Xing, B., 2011. Sorption of bisphenol a, 17α-ethinyl estradiol and phenanthrene on thermally and hydrothermally produced biochars. Bioresour. Technol. 102, 5757–5763. https://doi.org/10.1016/j.biortech.2011.03.038.

Tripathi, N., Hills, C.D., Singh, R.S., Atkinson, C.J., 2019. Biomass waste utilisation in low-carbon products: harnessing a major potential resource. NPJ Clim. Atmos. Sci. 2, 35. https://doi.org/10.1038/s41612-019-0093-5.

Vega, M.F., Díaz-Faes, E., Barriocanal, C., 2024. Kinetic and mechanistic study of CO_2 adsorption on activated hydrochars. J. CO2 Util. 81, 102716. https://doi.org/10.1016/j.jcou.2024.102716.

Wang, C., Fang, Y., Duan, H., Liang, G., Li, W., Chen, D., Long, M., 2021. DFT study of CO_2 adsorption properties on pristine, vacancy and doped graphenes. Solid State Commun. 337, 114436. https://doi.org/10.1016/j.ssc.2021.114436.

Wang, X., Chen, L., Guo, Q., 2015. Development of hybrid amine-functionalized MCM-41 sorbents for CO_2 capture. Chem. Eng. J. 260, 573–581. https://doi.org/10.1016/j.cej.2014.08.107.

Wickramaratne, N.P., Jaroniec, M., 2013. Activated carbon spheres for CO_2 adsorption. ACS Appl. Mater. Interfaces 5, 1849–1855. https://doi.org/10.1021/am400112m.

Yadav, T.R., Shrotri, A.R., Kate, P.N., Devasia, G., Niphadkar, P.S., Mali, N.A., Krishnamurty, S., Bokade, V.V., Nandanwar, S.U., 2025. Binderless low silica X zeolite for methane separation from binary CO_2/CH_4 biogas stream: a comprehensive experimental and computational study. J. Ind. Eng. Chem. 149, 705–719. https://doi.org/10.1016/j.jiec.2025.02.031.

Yogalakshmi, K.N., Poornima Devi, T., Sivashanmugam, P., Kavitha, S., Yukesh Kannah, S., Varjani, S., AdishKumar, S., Kumar, G., 2022. Lignocellulosic biomass-based pyrolysis: a comprehensive review. Chemosphere 286, 131824. https://doi.org/10.1016/j.chemosphere.2021.131824.

Yuan, X., Xiao, J., Yılmaz, M., Zhang, T.C., Yuan, S., 2022. N, P Co-doped porous biochar derived from cornstalk for high performance CO_2 adsorption and electrochemical energy storage. Sep. Purif. Technol. 299, 121719. https://doi.org/10.1016/j.seppur.2022.121719.

Zhang, T., Yuchi, W., Bai, Z., Hou, R., Feng, Z., Guo, Z., Kong, L., Bai, J., Meyer, B., Li, W., 2022. Insight into the charging methods effects during clean recycling of plastic by co-pyrolysis with low-rank coal. J. Clean. Prod. 333, 130168. https://doi.org/10.1016/j.jclepro.2021.130168.

Zhao, C., Ge, L., Li, X., Zuo, M., Xu, C., Chen, S., Li, Q., Wang, Y., Xu, C., 2023. Effects of the carbonization temperature and intermediate cooling mode on the properties of coal-based activated carbon. Energy 273, 127177. https://doi.org/10.1016/j.energy.2023.127177.

Zhu, Z., Tsai, H., Parker, S.T., Lee, J.-H., Yabuuchi, Y., Jiang, H.Z.H., Wang, Y., Xiong, S., Forse, A.C., Dinakar, B., Huang, A., Dun, C., Milner, P.J., Smith, A., Guimarães Martins, P., Meihaus, K.R., Urban, J.J., Reimer, J.A., Neaton, J.B., Long, J.R., 2024. High-capacity, cooperative CO_2 capture in a diamine-appended metal–organic framework through a combined chemisorptive and physisorptive mechanism. J. Am. Chem. Soc. 146, 6072–6083. https://doi.org/10.1021/jacs.3c13381.

Zou, R., Wang, C., Qian, M., Huo, E., Kong, X., Wang, Y., Dai, L., Wang, L., Zhang, X., Mateo, W.C., Ruan, R., Lei, H., 2022. Catalytic co-pyrolysis of solid wastes (low-density polyethylene and lignocellulosic biomass) over microwave assisted biochar for bio-oil upgrading and hydrogen production. J. Clean. Prod. 374, 133971. https://doi.org/10.1016/j.jclepro.2022.133971.